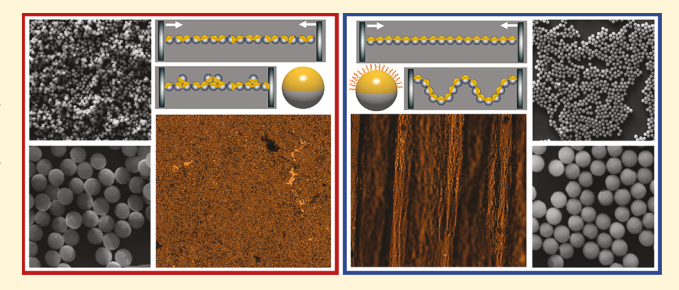
Impact of Surface Amphiphilicity on the Interfacial Behavior of Janus Particle Layers under Compression

Sepideh Razavi,**,†® Binhua Lin,‡® Ka Yee C. Lee,^{§®} Raymond S. Tu,^{®®} and Ilona Kretzschmar**,

Supporting Information

ABSTRACT: Langmuir monolayers of silica/gold Janus particles with two different degrees of amphiphilicity have been examined to study the significance of particle surface amphiphilicity on the structure and mechanical properties of the interfacial layers. The response of the layers to the applied compression provides insight into the nature and strength of the interparticle interactions. Different collapse modes observed for the interfacial layers are linked to the amphiphilicity of Janus particles and their configuration at the interface. Molecular dynamics simulations on nano-



particles with similar contact angles provide insight on the arrangement of particles at the interface and support our conclusion that the interfacial configuration and collapse of anisotropic particles at the air/water interface are controlled by particle amphiphilicity.

INTRODUCTION

Interfacial systems composed of fluids and surface-active materials have a wide range of applications in drug delivery, 1-3 food science,4-7 personal care products,8,9 and the chemical industry. The need to control the stability and functionality of these interfacial systems by tuning the type and properties of the stabilizing agent is self-evident. For example, the undesirable adsorption of proteins to fluid/fluid and fluid/solid interfaces during the processing of pharmaceutical products can be remediated by the addition of surfactants to the protein solution. 14 Another example is the potential to develop particle-stabilized reactive emulsions in which colloidal particles can be tuned for dual functionality; emulsion stabilization is achieved through particles binding to liquid/liquid interfaces, and reactivity is directed to a specific phase by selective functionalization of the particle surface.¹⁵ Therefore, these interfacial systems most often include surfactant molecules and/or colloidal particles. The binding of colloidal particles to fluid interfaces was discovered over a century ago by early experiments of Ramsden in 1904 and some 3 years later by Pickering. 16,17 Despite the century-old knowledge of this phenomenon, interest in a more fundamental understanding of the behavior of colloidal particles near interfaces has resurged in recent years 18,19 owing to the large binding energy that can be harnessed in emulsion and foam stabilization and the open nature of fluid interfaces that makes them a promising platform for applications in which the dynamics of transport is crucial.^{22,23} Whereas the initial body of work involved studies on

homogeneous spherical colloidal particles, the field has evolved to incorporate heterogeneous particles at interfaces, including shape anisotropic and surface anisotropic particles^{24,25} because of the recent boom in particle synthesis methods that has enabled the fabrication of anisotropic particles with designed heterogeneity. 26-32 The motivation behind the use of anisotropic particles at interfaces is to enhance the binding energy of the particle by maximizing the eliminated fluid/fluid interfacial area in the case of shape anisotropic particles and by increasing the difference in the wettability of polar and apolar regions (i.e., particle amphiphilicity) in surface anisotropic particles where the surface anisotropy can be induced physically through evaporation, chemically through exposure to a molecular ligand, or using a combination of both.^{33–36} Furthermore, the use of particulate building blocks with anisotropy in shape, surface characteristics, and/or chemical properties opens up access to functionalities that are difficult to replicate in systems solely stabilized by surfactants.^{37–39}

Particles with the proper wettability straddle fluid/fluid interfaces at an equilibrium contact angle (θ_E) that can be obtained from Young's equation by writing the balance of forces over the three-phase contact line (Figure 1a)

Special Issue: Intermolecular Forces and Interfacial Science

Received: June 1, 2019 Revised: July 3, 2019 Published: July 3, 2019



[†]Chemical, Biological, and Materials Engineering, University of Oklahoma, Norman, Oklahoma 73019, United States

 $^{^{\}ddagger}$ NSF's ChemMatCARS and the James Franck Institute and $^{\$}$ Department of Chemistry, Institute for Biophysical Dynamics, and the James Franck Institute, The University of Chicago, Chicago, Illinois 60637, United States

 $^{^{\}parallel}$ Department of Chemical Engineering, City College of the City University of New York, New York, New York 10031, United States

$$\cos \theta_{\rm E} = \frac{\gamma_{\rm po} - \gamma_{\rm pw}}{\gamma_{\rm ow}} \tag{1}$$

where $\gamma_{\rm ow}$ stands for the fluid/fluid surface tension and the surface tension of the particle in contact with the oil and water phases is denoted as $\gamma_{\rm po}$ and $\gamma_{\rm pw}$, respectively. The attachment energy of the particle to the interface can be derived from the change in the free energy of the system by going from state 1 (particle in the bulk phase) to state 2 (particle at the interface) as

$$\Delta E = -\pi R^2 \gamma_{\text{ow}} (1 - \cos \theta_{\text{E}})^2 \tag{2}$$

where R is the particle radius and $\theta_{\rm E}$ is the equilibrium contact angle of the particle at the interface as illustrated in Figure 1a. From this simple thermodynamic model, the binding strength of a 50 nm poly(methyl methacrylate) sphere at the hexadecane/water interface is estimated to be on the order of $10^5k_{\mathrm{B}}T^{.40}$ Therefore, colloidal particles with different wetting behavior, for example, polymeric vs inorganic particles, will yield different contact angles at the interface, which in turn gives rise to a change in the magnitude of the binding energy. Besides changing the particle type to tune the stability in interfacial systems, the addition of surfactant molecules to the particle suspension is another route to modifying the wettability and contact angle of particles at interfaces. For example, adding hexadecyltrimethylammonium bromide (CTAB) molecules to a suspension of silica nanoparticles has been shown to render the particles hydrophobic ($\theta_{\rm E} \approx$ 75°) at low CTAB concentrations with an enhanced binding energy of $\sim 10^3 k_{\rm B}T$, whereas increasing the CTAB concentration close to the critical micelle concentration causes the wettability of silica particles to revert back to hydrophilic ($\theta_{\rm E} \approx$ 25°) and reduces the magnitude of the binding energy at the air/water interface.4

Despite the large binding energy and high surface activity of homogeneous particles with a contact angle of $\theta_{\rm F} = 90^{\circ}$ at the interface, these particles are not amphiphilic, in contrast to surfactant molecules. Particles can be rendered amphiphilic by carrying out surface modifications on their two surface regions, designated here as polar (P) and apolar (A) as shown in Figure 1b. The position of the boundary between the polar and apolar regions on the particle surface is indicated by the angle α . The term Janus particle refers to a geometrically symmetric amphiphilic particle, a particle of anisotropic wettability with equal areas of the polar and apolar regions; (i.e., $\alpha = 90^{\circ}$). 42 The degree of amphiphilicity is then dictated by the difference in the wettability of the two faces and is defined as $\Delta\theta=\frac{\theta_{\rm A}-\theta_{\rm P}}{2}$, where $\theta_{\rm A}$ and $\theta_{\rm P}$ stand for the contact angle of the apolar and polar particles at the interface, respectively, as illustrated schematically in Figure 1b. The amphiphilicity of a particle can be tuned through the variation of both α (asymmetry of the surface) and the magnitude of the difference between the two contact angles, θ_P and θ_A . Zero amphiphilicity (the homogeneous case) corresponds to either $\alpha = 0^{\circ}$, $\alpha = 180^{\circ}$, or $(\theta_{\rm P} - \theta_{\rm A} = 0^{\circ})$, while the strongest amphiphilicity (Janus case) is expected when $\alpha = 90^{\circ}$ and $(\theta_{\rm P}$ $-\theta_{\rm A}=180^{\circ}$).

What is the impact of particle amphiphilicity on the interfacial configuration of a Janus particle? Does the particle straddle the interface with the Janus boundary aligned with the fluid interface? Similar to the derivation of the interfacial contact angle for homogeneous particles (eq 1), the

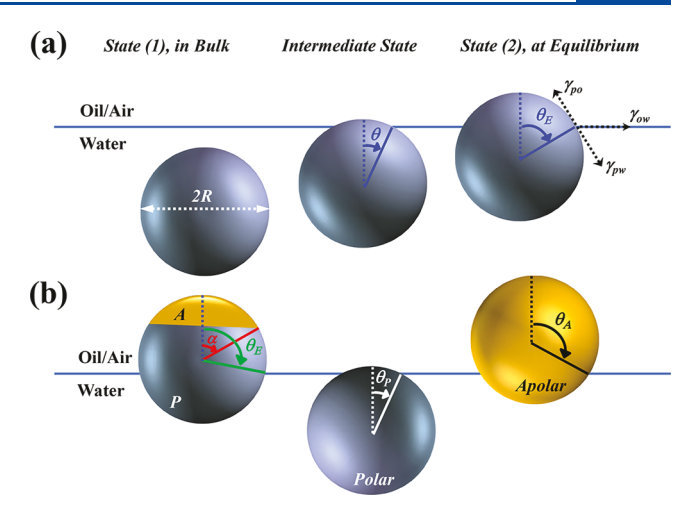


Figure 1. Schematics of (a) a homogeneous colloidal particle and (b) a heterogeneous particle with surface anisotropy characterized by the angle α separating the polar (P) and apolar (A) patches straddling a fluid/fluid interface. The immersion angle at equilibrium $(\theta_{\rm E})$ is dictated by the balance of surface energies at the three-phase contact line.

equilibrium position of an amphiphilic particle can be understood as the position that minimizes the total free energy composed of contributions from the fluid/solid and fluid/fluid interfacial energies; the former term in the surface energy favors maximizing the contact areas of the polar/apolar regions on the particle surface with their respective polar/apolar fluids, whereas the latter contribution favors a situation where the interface is intercepted by the largest cross-section of the solid sphere. Following the work of Ondarcuhu et al., ⁴³ the total surface energy, E, of an amphiphilic particle at a fluid/fluid interface as a function of the angle θ , which characterizes the immersion depth of the particle, can be written as

$$\begin{split} E(\theta) &= 2\pi R^2 \bigg[\gamma_{\text{Ao}} (1 + \cos \alpha) + \gamma_{\text{Po}} (\cos \theta - \cos \alpha) \\ &+ \gamma_{\text{Pw}} (1 - \cos \theta) - \frac{1}{2} \gamma_{\text{ow}} \sin^2 \theta \bigg] \quad \theta \leq \alpha \\ E(\theta) &= 2\pi R^2 \bigg[\gamma_{\text{Ao}} (1 + \cos \theta) + \gamma_{\text{Aw}} (\cos \alpha - \cos \theta) \\ &+ \gamma_{\text{Pw}} (1 - \cos \alpha) - \frac{1}{2} \gamma_{\text{ow}} \sin^2 \theta \bigg] \quad \theta \geq \alpha \end{split} \tag{3b}$$

where the surface tension of the polar region of the particle with either fluid phase is denoted as γ_{Po} and γ_{Pw} and the surface tension of the apolar region of the particle with either fluid phase is denoted as γ_{Ao} and γ_{Aw} , respectively. For a given amphiphilic particle, the values of θ_P , θ_A , and α are fixed and the minimization of the total interfacial energy with respect to the immersion angle, θ , yields the equilibrium contact angle of the particle at the interface, θ_E , with the following three possibilities

$$\theta_{\rm P} < \theta_{\rm A} < \alpha, \quad \theta_{\rm E} = \theta_{\rm A}$$
 (4a)

$$\theta_{\rm P} < \alpha < \theta_{\rm A}, \quad \theta_{\rm E} = \alpha$$
 (4b)

$$\alpha < \theta_{\rm p} < \theta_{\rm A}, \quad \theta_{\rm F} = \theta_{\rm p}$$
 (4c)

which highlights the importance of the wettability contrast between the two regions on a Janus particle and its

consequence with respect to the position of the particle at the interface. 44,45 Using the surface energy formulation of eq 3a for the case of a Janus particle with $\alpha = 90^{\circ}$, Binks et al. calculated the surface activity defined as the free energy required to desorb the particle from the interface into either of the bulk phases and concluded that enhancing the particle amphiphilicity can yield up to a 3-fold increase in desorption energies in comparison to those of homogeneous particles.⁴⁶ Following this prediction that suggests the potential application of Janus particles to more stable interfaces in multiphasic systems, a large body of work has been dedicated to theoretical studies, 47,48 simulations, 49-56 and experimental investigations⁵⁷⁻⁶² of Janus particles at fluid interfaces. In many of these studies, the change in interfacial tension of a fluid/fluid interface in the presence of particles is tracked as a function of time, and the results are compared between the homogeneous and Janus particles as an indicator of their interfacial activity. 63 For example, it was shown that gold/iron oxide Janus nanoparticles are considerably more effective at reducing the hexane/water interfacial tension than either gold or iron oxide homogeneous particles of comparable size and chemical nature.⁶⁴ Comparing the behavior of silver Janus nanoparticles with homogeneous poly(methyl methacrylate) or heterogeneously functionalized silica nanoparticles (with similar sizes of ~200 nm) revealed the remarkable interfacial activity of silver Janus nanoparticles at the decane/water interface where a 100fold higher concentration of either poly(methyl methacrylate) or silica was necessary to obtain a similar reduction of the interfacial tension as for the case of Janus nanoparticles.⁶ Similar results were obtained for Janus gold nanoparticles capped with half hexanethiol and half 2-(2-mercapto-ethoxy)ethanol at the air/water and decane/water interfaces, confirming their superior interfacial activity relative to that of the homogeneous gold nanoparticles.⁶⁶ The role of particle amphiphilicity in enhancing interfacial activity has been further validated in a system of pH-responsive Janus nanoparticles. 60 It has been shown that the interfacial activity of Janus nanoparticles is comparable to that of homogeneous nanoparticles when the amphiphilicity of the Janus nanoparticle is switched off, and when the amphiphilicity is switched on, the interfacial activity is enhanced. A more comprehensive review of recent studies on Janus particles at fluid interfaces can be found in refs 67-69.

The surface energy derivation of eq 3a assumes the behavior of a single amphiphilic particle at the interface without considering the rotational behavior of the particle. However, Monte Carlo simulations of Janus particles have shown that fixing the nanoparticle orientation leads to a significant increase in the nanoparticle-interface interaction strength; therefore, the nanoparticle's orientational freedom should not be neglected.⁷⁰ Assuming a flat interface, an analytical expression for the free energy as a function of orientation was derived by Stocco et al. for a single Janus particle.⁷¹ In addition, the interparticle interactions will also impact the configuration and collective behavior of particles in interfacial systems. Furthermore, fluid interfaces are not static but are constantly subject to external disturbances. In many applications relevant to particulate systems, the interface undergoes large deformations that produce compression and shear stresses; therefore, in addition to the physicochemical properties of particles, an effective stabilization heavily depends on the flow behavior of particles in response to applied deformations. 72-74 There is a need to study the stability of these interfacial systems in response to applied stresses in order to develop a better understanding of their dynamic behavior and performance in relevant applications. While most of the experimental and numerical work has been focused on the adsorption of Janus particles to fluid interfaces and their superior interfacial activity, less is known about their behavior in response to an applied stress.

Here, we investigate the question of how the change in Janus particle amphiphilicity impacts the interfacial configuration and mechanics by studying two sets of Janus particles ($\alpha=90^\circ$) with different degrees of amphiphilicity ($\Delta\theta$). We discuss the role that amphiphilicity plays in the microstructure of particle-laden interfaces and the resulting mechanical behavior and support our conclusions by carrying out molecular dynamics simulations on Janus nanoparticles.

MATERIALS AND METHODS

Janus Particle Fabrication. Silica (Fiber Optic Center, Inc.) particles with a nominal size of 1 μ m have been used in all experiments reported in this study. To tune the Janus particle amphiphilicity, two types of silica/gold Janus particles are fabricated; in one case, silica particles are half-coated with a 10-nm-thick gold layer through a 5-nm-thick adhesive titanium layer (Janus particles with a low degree of amphiphilicity), whereas in the other case, the gold coating is further modified with dodecanethiol molecules (Janus particles with a high degree of amphiphilicity). These two types of silica/gold Janus particles are referred to as JP_L and JP_H throughout the article. Details of the fabrication of Janus particles using the physical vapor deposition technique are provided in the Supporting Information. Using the density values for silica (2.0 g/cm³), titanium (4.5 g/cm³), and gold (19.2 g/cm³), and assuming that the Janus cap is crecent-shaped, 75 we estimate the density of a Janus particle to be 2.3 g/cm³. All glassware used in the study is thoroughly cleaned using a sulfuric acid (Certified ACS Plus, Fisher Scientific) and NOCHROMIX (Godax Laboratories, Inc.) mixture, followed by rinsing with copious amounts of ultrapure water and drying under vacuum. Water used throughout the study has a resistivity of 18.2 MΩ·cm and is obtained from an Advantage A10 Milli-Q System (EMD Millipore, Billerica, MA).

Contact Angle Measurements. To evaluate the amphiphilicity of the Janus particles, one needs to characterize the surface wettability of the two faces of the Janus particle (i.e., silica and gold for the JP_L particle and silica and thiolated gold for the JP_H particle). Three-phase contact angle measurements of a water droplet on an acid-cleaned glass slide and gold-coated glass slides are carried out to estimate the wettabilities on the silica and gold faces. Details of the experimental procedure are provided in the Supporting Information.

Langmuir Trough Measurements. A NIMA Langmuir trough with a working area of $A = 78 \text{ cm}^2$ is cleaned with chloroform and then filled with 65 mL of water. A paper Wilhelmy plate hanging from a pressure sensor is oriented parallel to the major axis of the barriers and measures the value of surface pressure (Π) , which is defined as the difference between the surface tension of the bare air/water interface (γ_0) and the effective surface tension of the particle-laden interface (γ) . To ensure the absence of any surface-active impurities, the interface is swept by closing the barriers to $A = 20 \text{ cm}^2$ and is aspirated several times until the surface pressure in the closed-barrier state is measured to be less than 0.2-0.3 mN/m. To prepare an interfacial film from each sample (unmodified silica particles, JP_L and JP_H Janus particles), different quantities of particles varying from 5 to 15 mg are dispersed in 200 μ L of a 70:30 wt % isopropyl alcohol (Certified ACS Plus, Fisher Scientific)/water mixture and sonicated for 2 min. The particles are placed at the air/water interface by careful drop-by-drop deposition of the dispersion using a 100 μ L Hamilton syringe, where spreading is driven by Marangoni flow. After waiting for 20 min to allow for evaporation of the spreading solvent, compression is carried out by reducing the trough area at 5 cm²/min, which corresponds to a linear barrier speed of 0.71 cm/min. During

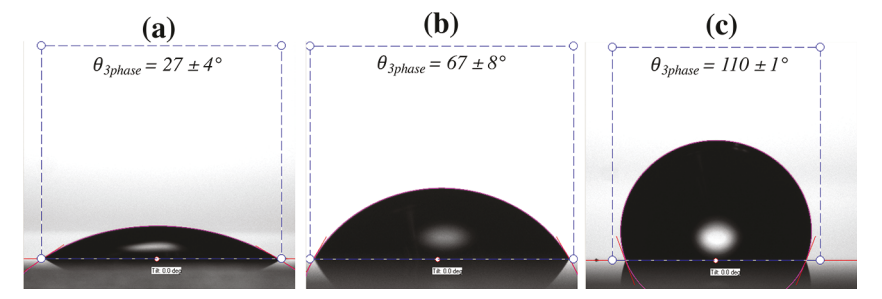


Figure 2. Macroscopic three-phase contact angle measurements of a water droplet in air and on (a) an acid-cleaned glass slide, (b) a gold-coated glass slide, and (c) a thiolated, gold-coated glass slide.

the compression—expansion cycle, the microstructure of the interfacial layer is captured using an Olympus BH-3 optical microscope with a $10\times$ objective and a charge-coupled-device (CCD) camera. Isotherm hysteresis is investigated by performing consecutive compression—expansion cycles, where compression is immediately followed by expansion of the monolayer. The static compression modulus (E_0) that captures the variations in interfacial tension resulting from changes in the interfacial area 76,77 is defined as

$$E_0 = -A \left(\frac{\partial \Pi}{\partial A} \right)_T = -\left(\frac{\partial \Pi}{\partial \ln A} \right)_T \tag{5}$$

and is evaluated to examine the impact of particle wettability on the strength and compressibility of the monolayers. To characterize the impact of particle amphiphilicity on the orientation of the Janus particle at the interface and the response of the particle layer to compression, interfacial monolayers of Janus particles formed at the air/water interface are transferred to a silicon wafer substrate from a Langmuir film using an inverse Langmuir—Schaefer deposition method.⁷⁸ The arrangement of the Janus cap in these layers is assessed via the EVO40 XVP scanning electron microscope from Zeiss. All experiments are carried out at room temperature.

Molecular Dynamics Simulations. Molecular dynamics simulations are employed to study the behavior of nanoscale Janus particles, specifically to examine the impact of particle amphiphilicity on the interfacial configuration of the particles at a fluid/fluid interface. The two-body interaction potential used in simulations is of the Lennard-Jones form

$$V_{\rm LJ}(r_{ij}) = 4\varepsilon \left[\left(\frac{\sigma}{r_{ij}} \right)^{12} - A_{\rm ss} \left(\frac{\sigma}{r_{ij}} \right)^{6} \right]$$
 (6)

where $r_{ij} = |{\bf r}_i - {\bf r}_j|$ is the distance between atomic centers for any two atoms (i,j=1,N) of species s and s', σ is the approximate diameter of an atom (the separation at which the short-distance repulsion begins to increase), and ϵ is the depth of the potential well at $r_{ij} = (2/A_{\rm ss'})^{1/6}\sigma$. For argon, the parameter values that fit the experiment are $\epsilon/k_{\rm B} \approx 120$ K and $\sigma \approx 0.32$ nm, and these, along with the mass of argon m=40 au, provide the natural atomic time scale $\tau=m(\sigma/\epsilon)^{1/2}\approx 2.2$ ps. All calculations are made using dimensionless variables with scaling parameters of σ (length scale), ϵ (energy scale), and m (mass of the fluid atoms).

The $A_{ss'}$ constant adjusts the strength of attraction between any two coexisting atomic species s and s' to tune the wettability of the particle surface. The simple Lennard-Jones model allows for isolation of the interfacial and capillary force effects, although it neglects the electrostatic interactions and gravity. The simulated systems reported here have five atomic species; fluid 1 (s=1), fluid 2 (s=2), the surrounding solid wall (s=3), and the solid particle with two hemispheres (s=4 and s=5). To model two macroscopically immiscible fluids, we set $A_{12}=A_{21}=0.5$ for cross-interactions and $a_{11}=a_{22}=1$ for self-interactions. Two bounding walls composed of atoms tethered to cubic lattice sites are used to confine the two fluids in the direction normal to the interface (y) and localize the interface in the center of

the simulation box. The interface is centered at y = 0 with periodic boundary conditions applied in the x and z directions. ^{79,80}

Particles used in these simulations are 4 nm in size. In simulating homogeneous nanoparticles, all atoms in the solid particle feel the same attraction/repulsion toward each fluid phase; therefore, the interaction coefficients used between the atoms in the particle and either fluids are the same for the lower (s=4) and upper (s=5) half of the particle. In contrast, the chemically anisotropic particles are composed of two different species on each hemisphere, and amphiphilicity is introduced by assigning different interaction coefficients to atoms in the lower (s=4) and upper (s=5) half of the particle. All calculations are made using an NVT ensemble, where the temperature is fixed at $T=1.0\epsilon/k_{\rm B}$ via a Nosé–Hoover thermostat and the density is set to $\rho=0.8/\sigma^3$. More information on the details of the simulation setup can be found in previously published work. 81,82

RESULTS AND DISCUSSION

Amphiphilicity of Janus Particles. To evaluate the wettability of silica and gold faces of the fabricated Janus particles, macroscopic contact angle measurements of water droplets are carried out on glass surfaces that went through identical surface modifications used for the Janus particles. It is noteworthy that these measurements are not an implication of the exact values of the particle's contact angle residing at the air/water interface but rather these values are used as a guide to compare the relative wettability of surfaces before and after modification. As shown in Figure 2, the average contact angle of water droplets on an acid-cleaned glass slide is measured to be $\theta_P = 27 \pm 4^{\circ}$, indicating the hydrophilic nature of the surface. The gold-coated surfaces exhibit a higher degree of hydrophobicity manifested by the droplet contact angle of θ_A = $67 \pm 8^{\circ}$ on the gold-coated glass slide and $\theta_{\rm A}$ = 110 \pm 1° on the thiolated gold surface. From these measurements and the definition of the degree of amphiphilicity, one can estimate $\Delta\theta = \frac{\theta_{\rm A} - \theta_{\rm P}}{2} \approx 20^{\circ}$ for JP_L and $\Delta\theta \approx 42^{\circ}$ for JP_H particles, where the degree of amphiphilicity is doubled in the latter case.

Response of Janus Layers to Compression. Homogeneous unmodified silica particles are used as a baseline for the systems of Janus particles studied here. The same protocol used for silica particles is employed to deposit Janus particles at the air/water interface and study the monolayer response to compression. The first noticeable change between the unmodified silica particles and Janus particles is the improved interfacial trapping for the Janus particle samples as depicted in the pressure isotherms provided in Figure 3. The figure illustrates a set of pressure isotherms for 7.5 mg of each particle type dispersed from 200 μ L of spreading solution onto the interface. On the basis of the estimated density of Janus particles (2.3 g/cm³), this quantity of particles amounts to

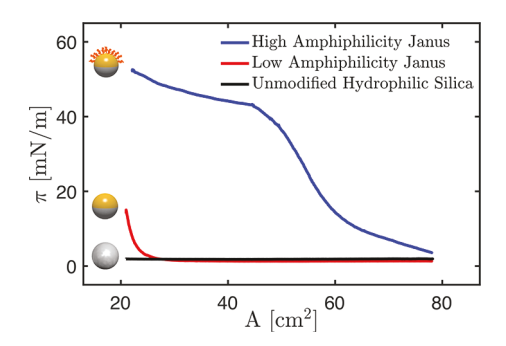


Figure 3. Pressure isotherms obtained for unmodified silica particles, Janus particles with low amphiphilicity (JP_L) , and Janus particles with high amphiphilicity (JP_H) . In all three experiments, 7.5 mg of each particle type was spread at the air/water interface.

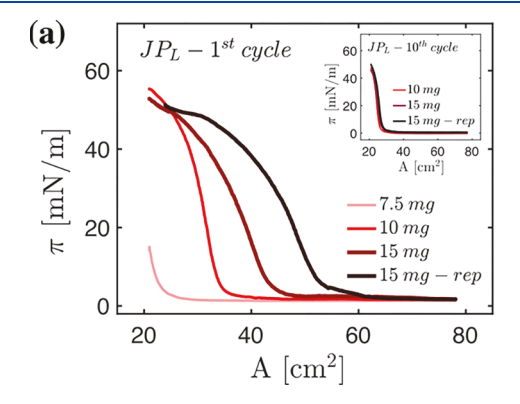
 \sim 6.1 \times 10⁹ Janus particles assuming the Janus cap is crescent-shaped.⁷⁵ It roughly corresponds to 1.27 μ m²/particle at the interface in the open-barrier state.

The lack of interfacial binding for unmodified silica particles is reflected in the zero surface pressure and the absence of any interfacial response to the applied changes in the surface area. This behavior has been attributed to the strong repulsion between the negatively charged silica particles and the interface.⁸³ In contrast, a pressure pickup is observed for both Janus particle types. The enhanced entrapment can be attributed to two factors: reduced repulsive interaction between the particle and the interface owing to the metal coating on half of the particle that covers the silanol groups and the introduced amphiphilicity on the surface of the particle which in turn increases the desorption energy from the interface. The latter impacts the effective particle entrapment at the interface for the two Janus particle types as evident in their different pressure isotherms. Using the same quantity of Janus particles in the spreading solution (e.g., 7.5 mg for the data presented in Figure 3), the pressure lift-off occurs at much larger trough areas for the JP_H monolayer compared to JP_L pointing to superior trapping of the former particle type with higher amphiphilicity.

To fully explore the behavior of both particle types at the interface, we present data on interfacial layers produced from a number of particle concentrations used in the spreading solution. The trough areas at closed- and open-barrier states are 21 and 78 cm², respectively. To reach a close-packed network of Janus particles in 2D at the interface (with a

packing fraction of 0.91 and an estimated Janus particle density of 2.3 g/cm³), we have calculated the number of required particles to be 2.4×10^9 (~3 mg) for the closed-barrier state and 9×10^9 (~11 mg) for the open-barrier state. To get these estimates, we have assumed a maximum air/water interfacial area removed per particle (πR^2) . On the basis of these estimates, we have examined the behavior of Janus particles using 5, 7.5, 10, and 15 mg of particles. The resulting pressure isotherms for both particle types are shown in Figure 4, and the corresponding microscopy images at different stages of compression and expansion are shown in Figure 5. In conjunction with the microscopy images, the pressure isotherms can be divided into five stages during a compression-expansion cycle: (I) after deposition, (II) inflection point of the isotherm, (III) onset of deformation out of the interface plane, (IV) monolayer collapse, and (V) expanded state with fully opened barriers. States I-IV are used to analyze the compression portion of the pressure isotherm, whereas state V occurs after the expansion is completed. It is worth pointing out that the dendritic structure of the interfacial layers formed by Janus particles (stage I shown in Figure 5ad) has been previously observed in both simulations⁸⁴ and experiments⁸⁵ and is attributed to the capillary interactions 56,86,87 in the presence of local deformations of the interface that stem from the rough Janus boundary.

As can be seen in Figure 4a, an interfacial layer of 7.5 mg JP_L particles does not exhibit a pronounced pressure increase over the range of compression applied. From Figure 5a, it can be seen that owing to the low population of particles trapped at the interface even in the fully compressed state accessible in the experiment, an inflection point, onset of deformation, and monolayer collapse are not observed. Increasing the number of IP_L particles in the spreading solution (10 and 15 mg) yields a highly populated interface, the compression of which results in isotherms that undergo an inflection point. The compression of layers beyond the inflection point leads to deformations that are out of the plane of the interface (i.e., collapse of the particle layer). Collapse of the JP_L layers occurs via the formation of a striation pattern followed by slight wrinkling of the layer as confirmed by the micrographs (Figure 5b). We speculate that particle contacts made by the applied compression are sticky and lead to the jammed state because of the strong van der Waals gold-gold interactions; therefore, particle rearrangements are not readily accessible upon expansion. In other words, JP_L monolayers are rigid and taking the particle layer to



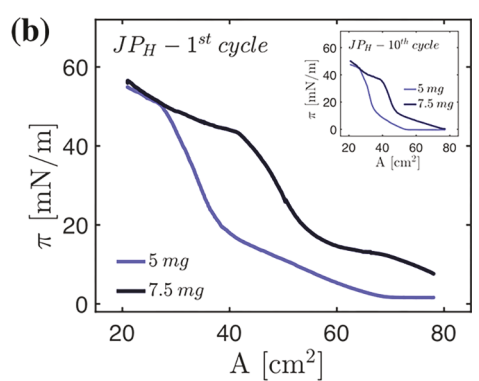


Figure 4. Impact of particle concentration on the pressure isotherms obtained for (a) Janus particles with a low degree of amphiphilicity (JP_L) and (b) Janus particles with a high degree of amphiphilicity (JP_H). The main figure and the insets show the isotherms for the 1st and 10th compression cycles, respectively. The varying number of particles used in the depositing solution and the replicate experiment are denoted in the legend.

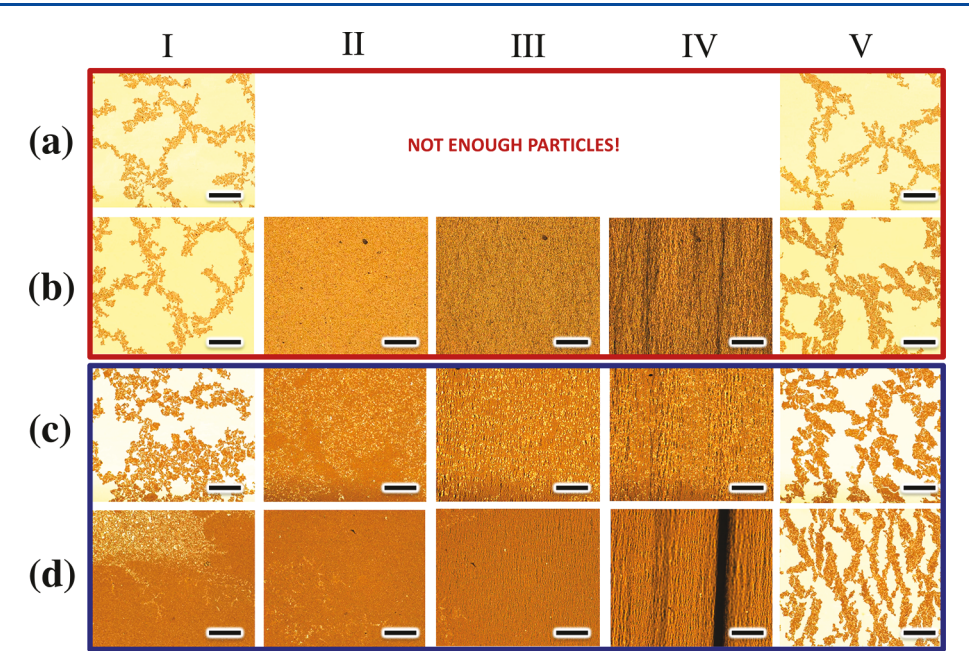


Figure 5. Optical images of Janus-particle-laden air/water interfaces prepared using spreading solutions that contain (a) 7.5 mg of $JP_{L^{\prime}}$ (b) 10 mg of $JP_{L^{\prime}}$ (c) 5 mg of $JP_{H^{\prime}}$ and (d) 7.5 mg of $JP_{H^{\prime}}$ and (d) 7.5 mg of $JP_{H^{\prime}}$ captured at different stages of the compression—expansion cycle: (I) after deposition, (II) inflection point, (III) onset of deformations out of the interfacial plane, (IV) monolayer collapse, and (V) expanded state with fully opened barriers. All scale bars are 200 μ m.

Table 1. Number of Particles Deposited at the Interface in Each Experiment, with the Corresponding Trapped Particles at the Interface Calculated from the Area at Which the Isotherm Undergoes Inflection for the 1st and 10th Cycles^a

particle	deposited (mg)	deposited no.	trapped no. (1st cycle)	entrapment efficacy (%)	trapped no. (10th cycle)	percentage lost (%)
$\mathrm{JP_{L}}$	7.5	6.1×10^9	NA	<40	NA	NA
	10	8.2×10^9	3.6×10^9	44	2.8×10^{9}	22
	15	12.3×10^9	4.4×10^9	36	2.8×10^{9}	36
	15 (replica)	12.3×10^9	5.5×10^9	45	2.9×10^{9}	46
JP_{H}	5	4.1×10^9	3.8×10^{9}	93	3.6×10^9	4.6
	7.5	6.1×10^9	5.7×10^9	92	5.1×10^9	10.1

"The entrapment efficacy for each particle type is calculated on the basis of the deposited and estimated trapped number of particles at the interface. The % lost during successive deformations is calculated from the estimated number of particles in the 1st and 10th cycles. NA refers to not accessible.

a highly compressed state beyond the inflection point leads to the collapse of the layer through irreversible out-of-plane deformations. The irreversible nature of these contacts is corroborated by the isotherm hysteresis observed between successive cycles. From Figure 4a, it is apparent that the pressure isotherms have different slopes initially during the first cycle. Even two replicate experiments using the same particle concentrations to make a monolayer (isotherms for 15 mg JP_L) might have different responses to the applied compression. This behavior can be related to the efficacy of particle entrapment at the interface and the contacts made with neighbors as the particles are trapped at the interface. However, through successive compressions, the isotherms gradually shift closer and eventually line up after 10 cycles (inset of Figure 4a). At this point, the particle layer is no longer a 2D monolayer but rather a disordered particle film with a 3D structure and a modulus of 310 \pm 34 mN/m that sustains \sim 50 mN/m pressure. The low slope of pressure isotherms for monolayers of 10 and 15 mg particles on the first cycle (modulus of 205 \pm 52 mN/m) sharpens after 10 cycles, pointing to the higher modulus of the 3D particle film owing to its increased thickness.

Using the inflection point of the isotherm and identifying the area at which the onset of out-of-plane deformations are observed during the first compression—expansion cycle, we estimate the actual number of particles present at the interface assuming hexagonal close packing. The number of particles corresponding to each mass is provided in Table. 1. We then compare the number of trapped particles for each case to the number of particles deposited at the interface from the spreading solution to assess the entrapment efficacy of the Janus particles, especially the impact of the degree of amphiphilicity on the particle binding at the interface.

From the area at the inflection point during the 10th cycle, we can estimate the number of particles that are still present at the interface after 10 compressions and expansions. By contrasting this value with the number calculated for the 1st cycle, we can arrive at the percentage of particles lost as a result of the successive compression—expansion cycles. This value highlights the impact of amphiphilicity on the particle interfacial stability when subjected to deformations. Whereas this value is $\sim\!10\%$ or less for JP_H particles as illustrated in Figure 4b, it ranges from 22 to 46% for the JP_L particles. Assuming that all lost particles have been incorporated into

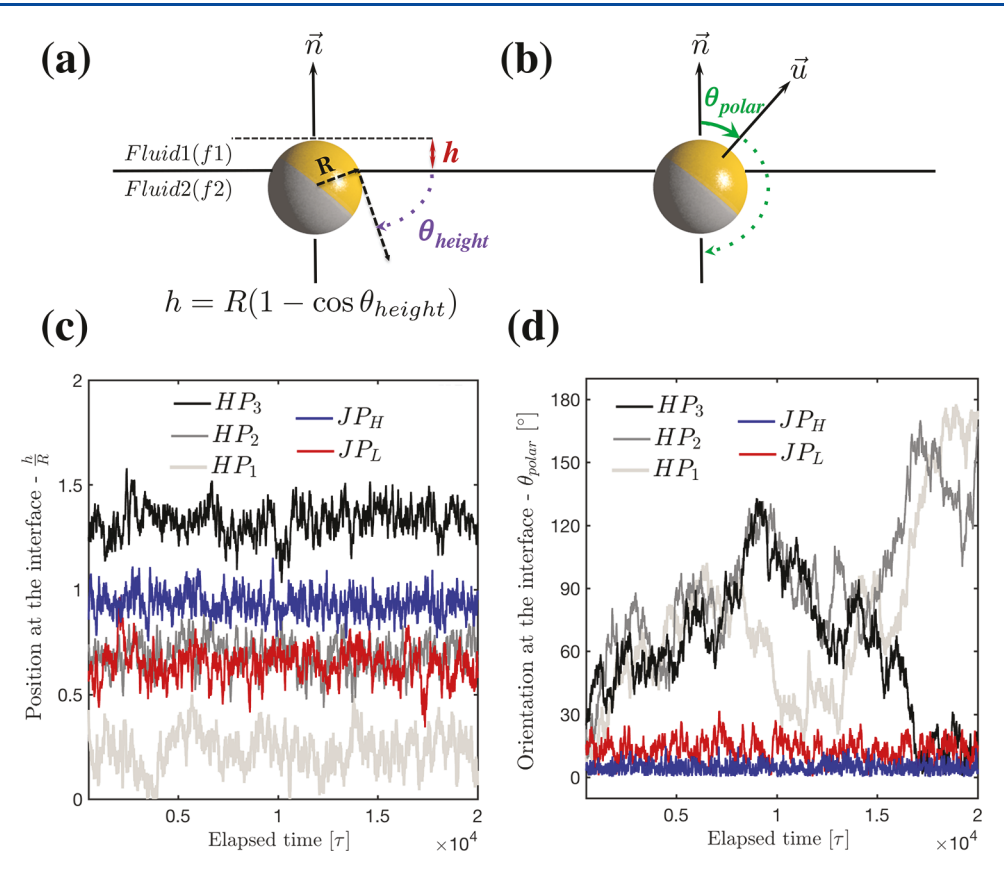


Figure 6. (a, b) Interfacial configuration of a Janus particle described using two angles: (a) θ_{height} representing the particle height at the interface, h, and (b) θ_{polar} showing the Janus cap orientation. (c, d) Simulation results illustrating the (c) translational and (d) rotational trajectories of homogeneous nanoparticles HP₁, HP₂, and HP₃ with different surface wettabilities compared to the dynamics of Janus nanoparticles with low (JP_L) and high degrees of amphiphilicity (JP_H).

secondary layers without any loss to the subphase, this quantity of desorbed particles corresponds to 0.26, 0.51, and 0.78 coverage as a secondary layer. It should be noted that particles might not necessarily be in one secondary layer on top of the primary interfacial layer but could be forming tertiary layers and beyond.

The amphiphilicity and surface properties of Janus particles play consequential roles in the structure of the interfacial layer and the ensuing collapse mode. Isotherms of Figure 4 illustrate that pressure lift-off and collapse can be accessed using a lower particle concentration for JPH in comparison to that for JPL, hinting at a more pronounced trapping for the former, more amphiphilic case. Whereas spreading a solution of 7.5 mg of JP_L particles is not sufficient to reach an inflection point in the isotherm, 5 mg of JP_H particles results in a dense layer that eventually collapses at about 50 mN/m. The collapse of JP_H particle layers takes place through buckling (Figure 5c, IV) and folding (Figure 5d, IV), which are reversible in contrast to the JP_L case. Folds and wrinkles open upon expansion without any material loss to irreversible 3D particle film formation as confirmed by the slope and shape of the isotherms in comparing the 1st and 10th cycles (Figure 4b and inset). While the densification of the particulate structures leads to a gradual increase in slope for successive cycles for JP_I, the slope of the pressure isotherm for JP_H remains low even after 10 cycles with a characteristic modulus of 167 \pm 4 mN/m at the inflection point of the isotherm.

Amphiphilicity and Interfacial Configuration. On the basis of our findings on the response of Janus particle layers to

compression and the accompanying micrographs, we postulate that the attractive interparticle interactions are softer in the case of JP_H particles; therefore, collapse of the layer is reversible where the JP_H monolayer recovers its 2D dendritic structure at the interface upon expansion. We argue that the distinct collapse modes observed are influenced by the impact of amphiphilicity on the particle configuration and resulting interparticle interactions. It should be noted that the amphiphilicity will impact the height of the particle residing at the interface, which in turn affects the interparticle interactions and resulting orientation at the interface. Additionally, the configuration of the particle at the interface will dictate the medium through which the interparticle interactions are taking place (air vs. water subphase) and will therefore affect the type and strength of interparticle interactions including van der Waals and electrostatic interactions. Here, we have attributed our observations to the difference in amphiphilicity $(\Delta \theta)$ without a detailed investigation of how each type of interaction is altered when we modify the particle amphiphilicity from JP_L to JP_H. The difference in amphiphilicity has consequences for the particle entrapment at the interface (Table. 1) and the interfacial configuration of the trapped particles (i.e., particle position (h) and particle orientation (θ_{polar}) at the interface (Figure 6a,b)). The height (h) of the particle residing at the interface can be converted to the particle contact angle denoted by θ_{height} , which refers to the equilibrium contact angle of the particle at the interface $(\theta_{\rm E})$ as discussed in eq 1 for homogeneous particles and in eq 4a for Janus particles.

Table 2. Interaction Potential Coefficients $(A_{ss'})$ between the Particle and the Two Fluids Used in the Simulations and the Position of the Resulting Homogeneous Nanoparticles at the Interface^a

nanoparticle	$A_{ m ss'}$	h/R	$ heta_{ ext{height}}$ (deg)	surface analogue	$ heta_{3 ext{phase}}$ (deg)
HP_1	$A_{\rm f1P} = 0.75$	0.23 ± 0.09	39 ± 8	silica	27 ± 4
	$A_{\rm f2P} = 0.25$				
HP_2	$A_{\rm f1P}=0.6$	0.68 ± 0.07	72 ± 4	gold	67 ± 8
	$A_{\rm f2P}=0.4$				
HP_3	$A_{\rm f1P}=0.4$	1.33 ± 0.07	109 ± 4	thiolated gold	110 ± 1
	$A_{\rm f2P} = 0.6$				

^aThe experimental analogs and their respective three-phase contact angle are also provided for comparison.

To shed light on the role of particle amphiphilicity in the orientation of Janus particles at the interface and the resulting interactions with neighboring particles, we have carried out MD simulations with 4 nm particles. We use the three-phase contact angle (θ_{3phase}) measurements of Figure 2 as a guide to determine the choice of interaction coefficients $A_{ss'}$. In other words, we run a set of simulations for a homogeneous nanoparticle (HP) straddling a fluid interface and adjust the interaction coefficients until we obtain three-phase contact angles that are analogous to those measured experimentally for unmodified silica, gold, and thiolated gold. The interaction potential coefficients found for the three homogeneous nanoparticles and their resulting contact angle at the interface are summarized in Table. 2. The simulated homogeneous nanoparticles are labeled HP₁ (silica), HP₂ (gold), and HP₃ (thiolated gold).

We then combine the identified interaction coefficients in pairs in order to build a Janus particle. The atoms located in the bottom hemisphere of the particle represent the base of a Janus particle, and the atoms in the top hemisphere mimic the Janus cap. Therefore, to imitate the wettability of JP_L Janus particles, the interaction potential of HP₁ is employed for the atoms in the base of the particle, and the one found for HP₂ is used for the atoms in the Janus cap. Analogously, to build a Janus particle with high amphiphilicity, JP_H, the interaction potentials of HP₁ and HP₃ are combined. A single nanoparticle is then placed randomly at the interface to find its equilibrium position. After equilibrating the system for 500τ , the position and orientation of the particle at the interface are recorded as a function of time to capture the interfacial dynamics of each particle type.

The dynamic interfacial configuration of the simulated homogeneous and Janus nanoparticles is displayed in Figure 6c,d. The interfacial position of JP_L (red trace) is very similar to that of the homogeneous nanoparticle from which the Janus cap is created, namely, HP₂ (medium gray), a behavior that originates from the low amphiphilicity of the Janus particle (Figure 6c). In contrast, the high amphiphilicity of JP_H (blue trace) leads to complete immersion of the Janus cap in the top fluid with $h/R \approx 1$, corresponding to θ_{height} contact angles that are hovering around 90°. Snapshots of the simulations on the interfacial configuration of Janus particles are illustrated in Figure 7; the top fluid is not shown to make the interfacial position of the particles more visible. JP_L sits at the interface with the Janus boundary lower than the interface height, whereas the Janus boundary is aligned with the interface for JP_H. While restricted translational diffusion of Janus particles in the plane and out of the plane of the interface has been reported in the literature, 88 the more interesting observation is related to the orientation of these particles and their rotational freedom at the interface (Figure 6d). Simulation studies have

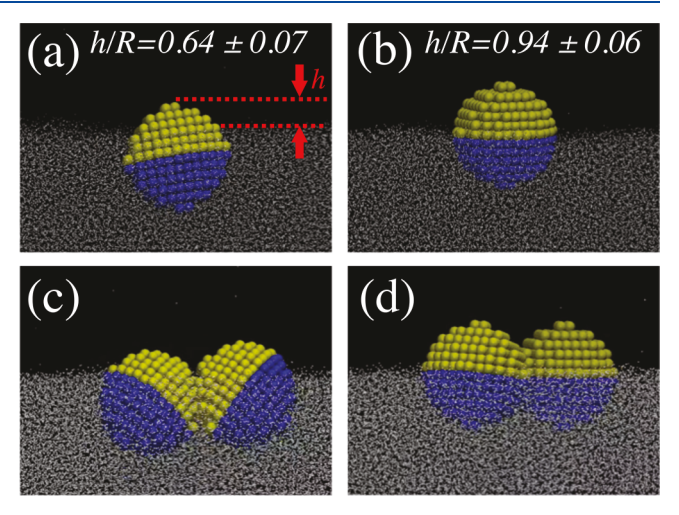


Figure 7. Snapshots of the molecular dynamics simulations showing the interfacial configuration of a single Janus particle and a pair of Janus particles at the interface. (a, c) Particles with low degree of amphiphilicity, JP_L , and (b, d) particles with high degree of amphiphilicity, JP_H .

shown that rotational diffusion parallel to the plane of the interface becomes slower upon increasing the amphiphilicity. Here, we demonstrate that both Janus particles also possess restricted rotational freedom perpendicular to the plane of the interface in contrast to homogeneous particles that rotate freely at the interface as expected. The restricted orientational freedom is expected for JP $_{\rm H}$ owing to its high amphiphilicity; however, the rotational behavior of JP $_{\rm L}$ is different from that of both HP $_{\rm 1}$ (light gray trace) and HP $_{\rm 2}$ despite the similarity in its interfacial position with respect to HP $_{\rm 2}$ (Figure 6c), implying that even low amphiphilicity gives rise to restricted out-of-plane rotations.

To connect the behavior of a single particle to the collective behavior of Janus particles at an interface, pairs of Janus particles are also studied. For these simulations, the interactions between particles need to be set as well (i.e., the strength of the cap—cap interaction compared to that of cap—base and base—base interactions). Our previous study on Langmuir trough measurements of unmodified silica particles illustrates that the silica—silica interactions are not attractive, so thus the interaction coefficient, $A_{ss'}$, between the base of the particles is set to zero (eq 6). To set the other two coefficients (cap—cap and cap—base), we use the data available in the literature on the value of Hamaker constants. For gold/gold and gold/silica surfaces interacting through water as the medium, the Hamaker constants are computed as 2.35 and 1.27 eV, respectively. Because the van der Waals interactions are almost twice as strong between gold surfaces

in comparison to those between gold and silica surfaces, the interaction coefficient between the two gold caps is set to A=1 in simulations, while the cap—base interaction coefficient is chosen to be A=0.5.

In simulating a pair of Janus particles, two particles are randomly placed at the interface and are allowed to move freely for 500τ to find their equilibrium configuration. The interfacial configurations for Janus particle pairs resulting from simulating JP_L and JP_H Janus particles are shown in Figure 7b. The cap-cap attraction causes particle rearrangement to a tilted orientation in JP_L, particles with low amphiphilicity. In comparison, for JP_H particles, the higher degree of amphiphilicity keeps the particles in their upright cap orientation with regard to the interface where the particles interact by aligning their caps side by side. Inspired by these simulation results, we examined the structure of the interfacial layers to investigate the impact of particle amphiphilicity on the interfacial configuration in the experiments with micrometer-sized particles. The particle layers are deposited on a silicon wafer at the end of the Langmuir trough measurements followed by examination with a scanning electron microscope. Images of both particle layers after compression are displayed in Figure 8 at two different magnifications. Whereas the

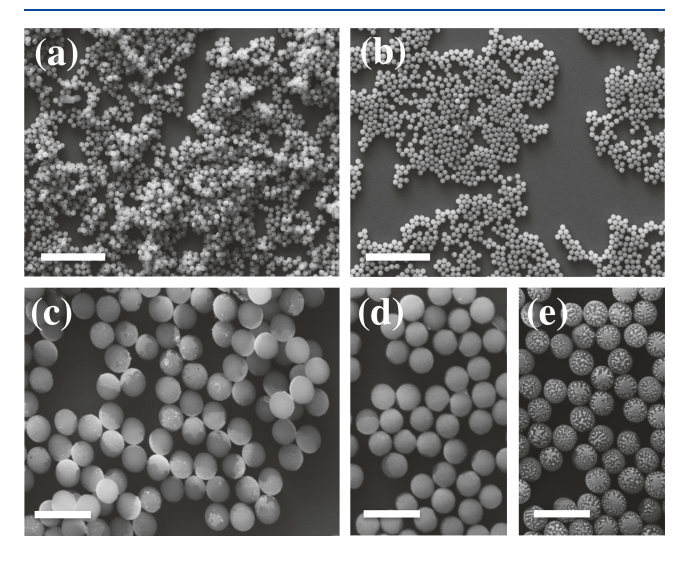


Figure 8. SEM images of Janus particle layers after the compression experiments: (a, c) Janus particles of low amphiphilicity (JP_L) and (b, d) Janus particles of high amphiphilicity (JP_H); the former particle type exhibits multilayer formation, whereas the latter remains as a monolayer. (e) Imaging the JP_H particle layer after 6 months demonstrates the dewetting of the gold coating, which further corroborates the cap-up orientation of these particles at the interface. (a, b) Scale bars are 10 μm and (c–e) scale bars are 2 μm .

structure formed by JP_L particles is 3D and disordered (Figure 8a), the appearance of the JP_H particle layer confirms its 2D nature (Figure 8b) and the fact that this particle type remains in a single layer even after undergoing 15 compression—expansion cycles. The higher-magnification images of each particle layer provide insight into the interfacial configurations of both particle types. In Figure 8c, a large number of gold contacts can be easily identified from the brighter appearance of gold in comparison to silica, and it can be concluded that a significant number of JP_L particles reside sideways at the interface, a finding in good agreement with the MD simulations and previous studies.

of this particle layer is thus attributed to the formation of "sticky" gold-gold contacts. In comparison, the brightness of the SEM images taken from the JP_H layer does not exhibit a noticeable variation across the image (Figure 8d), thus the particles are lined up with their gold side pointing up (toward the air phase). Another observation that supports the upright orientation of JP_H particles is the dewetting of the gold side that takes place on the surface of the JP_H particles and is visible after rescanning the same wafer after 6 months of storage (Figure 8e). Interestingly, the dewetting process is not observed for JP_L particles despite both caps having the same titanium adhesive layer. Previous work has shown that the diffusion of gold atoms is an activated process and the presence of self-assembled thiol molecules on gold substrates reduces the activation barrier and enables the mobility of gold atoms at room temperature. 95-97 We hypothesize that the observed dewetting in JP_H particles is related to the enhanced mobility of gold atoms in the presence of thiol molecules for this particle type.

The combination of Langmuir trough experiments and MD simulations allows us to conclude that the amphiphilicity of Janus particles plays a crucial role in their interfacial configuration, mechanical properties under applied stresses, and the ensuing collapse mode. These findings suggest that the nature of the particle surface can be precisely engineered to control the stability of a fluid/fluid interface. Further experiments need to be carried out to closely examine the collapse mode by gradually changing the particle amphiphilicity. These sets of experiments will explore the transition from the irreversible collapse (for the case of particles with a low degree of amphiphilicity) to a reversible wrinkling (for the case of particles with a high degree of amphiphilicity). Additionally, the impact that a change in amphiphilicity may have on the resulting interparticle interactions, especially electrostatic interactions, needs to be investigated and can be probed using an electrolyte-rich subphase. These topics are the subject of an ongoing study.

CONCLUSIONS

This article provides a study of interfacial colloidal monolayers formed from Janus particles with two different degrees of amphiphilicity. The significance of particle surface properties and amphiphilicity with regard to the interfacial configuration of particles and the mechanical strength of the resulting monolayers are highlighted. MD simulations show that introducing amphiphilicity into the particle leads to a more restricted rotational motion (out of the plane of the interface) in comparison to that for homogeneous particles. However, the interfacial position of Janus particles with a low degree of amphiphilicity is dictated by the wettability of the cap and not the Janus boundary. Examining the impact of interparticle interactions revealed that Janus particles of low amphiphilicity can reside at the interface in sideways orientation and are not pinned at the Janus boundary, whereas increasing the degree of amphiphilicity gave rise to the cap-up orientation of particles at the interface. Simply introducing amphiphilicity into a particle does not give rise to Janus behavior where the particle straddles the interfaces with the Janus boundary aligned with the interface. The interfacial configuration of particles in each case proved consequential in the response of particle layers to applied compressions in a Langmuir trough. It is found that particles with a low degree of amphiphilicity form a stiff, porous 3D film at the interface as a result of the random

orientation of particles at the interface, whereas particles with a higher degree of amphiphilicity gave rise to a soft elastic monolayer at the interface that collapses via reversible wrinkles and folds when subjected to compression. In summary, our results provide insight into the consequential role of the particle surface properties and amphiphilicity in the behavior of Janus particles at fluid/fluid interfaces and are highly relevant to experiments in the areas of Pickering emulsions and interfacially templated materials.

ASSOCIATED CONTENT

S Supporting Information

The Supporting Information is available free of charge on the ACS Publications website at DOI: 10.1021/acs.langmuir 9b01664

Janus particle fabrication and contact angle measurements (PDF)

AUTHOR INFORMATION

Corresponding Authors

*E-mail: srazavi@ou.edu.

*E-mail: kretzschmar@ccny.cuny.edu.

ORCID

Sepideh Razavi: 0000-0003-1225-6081 Binhua Lin: 0000-0001-5932-4905 Ka Yee C. Lee: 0000-0003-0895-336X Raymond S. Tu: 0000-0002-6192-7665 Ilona Kretzschmar: 0000-0001-7636-1679

Notes

The authors declare no competing financial interest.

ACKNOWLEDGMENTS

This work was supported by the National Science Foundation through award CBET-1067501, the MRSEC program at the University of Chicago (DMR-1420709), and the Air Force Office of Scientific Research (AFOSR no. FA9550-14-1-0263). B.L. acknowledges partial support from the NSF (CHE-1834750). K.Y.C.L. acknowledges support from the NSF (MCB-1413613). S.R. acknowledges partial funding from the NSF PREM program (DMR-0934206) and support from the office of the Vice President for Research and the Provost's office at the University of Oklahoma and thanks Prof. Joel Koplik for providing the initial version of the code used for the MD simulations. We would like to dedicate this article to Jacob N. Israelachvili, who has and continues to inspire us with his visionary work on interfacial forces.

REFERENCES

- (1) Chertok, B.; Webber, M. J.; Succi, M. D.; Langer, R. Drug delivery interfaces in the 21st century: from science fiction ideas to viable technologies. *Mol. Pharmaceutics* **2013**, *10*, 3531–3543.
- (2) Tadros, T. Colloid and Interface Science in Pharmaceutical Research and Development; Ohshima, H., Makino, K., Eds.; Elsevier: Amsterdam, 2014; Chapter 2, pp 29–54.
- (3) Dasgupta, S.; Auth, T.; Gompper, G. Nano- and microparticles at fluid and biological interfaces. *J. Phys.: Condens. Matter* **2017**, *29*, 373003.
- (4) Israelachvili, J. The science and applications of emulsions an overview. *Colloids Surf., A* **1994**, *91*, 1–8.
- (5) Berton-Carabin, C. C.; Sagis, L.; Schroën, K. Formation, Structure, and Functionality of Interfacial Layers in Food Emulsions. *Annu. Rev. Food Sci. Technol.* **2018**, *9*, 551–587.

(6) Linke, C.; Drusch, S. Pickering emulsions in foods opportunities and limitations. *Crit. Rev. Food Sci. Nutr.* **2018**, *58*, 1971–1985.

- (7) Green, A. J.; Littlejohn, K. A.; Hooley, P.; Cox, P. W. Formation and stability of food foams and aerated emulsions: Hydrophobins as novel functional ingredients. *Curr. Opin. Colloid Interface Sci.* **2013**, 18, 292–301.
- (8) Colloids in Cosmetics and Personal Care: Colloids and Interface Science; Tadros, T. F., Ed.; Wiley-VCH Verlag GmbH & Co. KGaA, 2011, Vol. 4.
- (9) Gkotsis, G.; Rickard, J. J. S.; Brooker, A.; Bakalis, S.; Grover, L. M.; Oppenheimer, P. G. Fabrication of optimized skin biomimics for improved interfacial retention of cosmetic emulsions. *J. R. Soc., Interface* **2018**, *15* DOI: 10.1098/rsif.2018.0332.
- (10) Aman, Z. M.; Koh, C. A. Interfacial phenomena in gas hydrate systems. *Chem. Soc. Rev.* **2016**, *45*, 1678–1690.
- (11) He, L.; Lin, F.; Li, X.; Sui, H.; Xu, Z. Interfacial sciences in unconventional petroleum production: from fundamentals to applications. *Chem. Soc. Rev.* **2015**, *44*, 5446–5494.
- (12) Chakma, A. Interfacial phenomena in petroleum recovery, edited by Morrow, N. R. Can. J. Chem. Eng. 1993, 71, 493-494.
- (13) Peng, B.; Zhang, L.; Luo, J.; Wang, P.; Ding, B.; Zeng, M.; Cheng, Z. A review of nanomaterials for nanofluid enhanced oil recovery. *RSC Adv.* **2017**, *7*, 32246–32254.
- (14) Khan, T. A.; Mahler, H.-C.; Kishore, R. S. K. Key interactions of surfactants in therapeutic protein formulations: A review. *Eur. J. Pharm. Biopharm.* **2015**, *97*, 60–67.
- (15) Crossley, S.; Faria, J.; Shen, M.; Resasco, D. E. Solid Nanoparticles that Catalyze Biofuel Upgrade Reactions at the Water/Oil Interface. *Science* **2010**, 327, 68–72.
- (16) Ramsden, W.; Gotch, F. Separation of solids in the surface-layers of solutions and 'suspensions' (observations on surface-membranes, bubbles, emulsions, and mechanical coagulation).-Preliminary account. *Proc. R. Soc. London* **1904**, *72*, 156–164.
- (17) Pickering, S. U. CXCVI.-Emulsions. J. Chem. Soc., Trans. 1907, 91, 2001–2021.
- (18) Snoeyink, C.; Barman, S.; Christopher, G. F. Contact Angle Distribution of Particles at Fluid Interfaces. *Langmuir* **2015**, *31*, 891–897.
- (19) Maestro, A.; Guzmán, E.; Ortega, F.; Rubio, R. G. Contact angle of micro- and nanoparticles at fluid interfaces. *Curr. Opin. Colloid Interface Sci.* **2014**, *19*, 355–367.
- (20) Destribats, M.; Gineste, S.; Laurichesse, E.; Tanner, H.; Leal-Calderon, F.; Héroguez, V.; Schmitt, V. Pickering Emulsions: What Are the Main Parameters Determining the Emulsion Type and Interfacial Properties? *Langmuir* **2014**, *30*, 9313–9326.
- (21) Kim, D.; Krishnamoorti, R. Interfacial Activity of Poly[oligo-(ethylene oxide)-monomethyl ether methacrylate]-Grafted Silica Nanoparticles. *Ind. Eng. Chem. Res.* **2015**, *54*, 3648–3656.
- (22) Lin, Y.; Skaff, H.; Emrick, T.; Dinsmore, A. D.; Russell, T. P. Nanoparticle Assembly and Transport at Liquid-Liquid Interfaces. *Science* **2003**, 299, 226–229.
- (23) Song, Y.; Chen, S. Janus Nanoparticles as Versatile Phase-Transfer Reagents. *Langmuir* **2014**, *30*, 6389–6397.
- (24) Park, B. J.; Lee, D. Particles at fluid-fluid interfaces: From single-particle behavior to hierarchical assembly of materials. *MRS Bull.* **2014**, 39, 1089–1098.
- (25) Morris, G.; Hadler, K.; Cilliers, J. Particles in thin liquid films and at interfaces. *Curr. Opin. Colloid Interface Sci.* **2015**, 20, 98–104.
- (26) Liang, F.; Zhang, C.; Yang, Z. Rational Design and Synthesis of Janus Composites. *Adv. Mater.* **2014**, *26*, 6944–6949.
- (27) Niu, X.; Ran, F.; Chen, L.; Lu, G. J.-E.; Hu, P.; Deming, C. P.; Peng, Y.; Rojas-Andrade, M. D.; Chen, S. Thermoswitchable Janus Gold Nanoparticles with Stimuli-Responsive Hydrophilic Polymer Brushes. *Langmuir* **2016**, *32*, 4297–4304.
- (28) Yu, B.; Cong, H.; Peng, Q.; Gu, C.; Tang, Q.; Xu, X.; Tian, C.; Zhai, F. Current status and future developments in preparation and application of nonspherical polymer particles. *Adv. Colloid Interface Sci.* 2018, 256, 126–151.

(29) Ghosh, S.; Schurtenberger, P. Microfluidic production of snowman-shaped Janus hydrogel particles. *Colloids Surf., A* **2019**, *573*, 205–210

- (30) Wang, K.; Wang, G.; Lu, C. Particle contact angle at the oilwater interface: Effect of surface silanization. *Particuology* **2019**, *44*, 218–224.
- (31) Zhai, W.; Song, Y.; Gao, Z.; Fan, J.-B.; Wang, S. Precise Synthesis of Polymer Particles Spanning from Anisotropic Janus Particles to Heterogeneous Nanoporous Particles. *Macromolecules* **2019**, *52*, 3237–3243.
- (32) Tan, J. S. J.; Chen, Z. Mask-less preparation of Janus particles through ultraviolet irradiation on hydrophobic particles assembled at the air-water interface. *J. Colloid Interface Sci.* **2019**, *546*, 285–292.
- (33) Maestro, A.; Santini, E.; Guzmán, E. Physico-chemical foundations of particle-laden fluid interfaces. *Eur. Phys. J. E: Soft Matter Biol. Phys.* **2018**, *41*, 97.
- (34) Park, B. J.; Lee, D. Configuration of nonspherical amphiphilic particles at a fluid-fluid interface. *Soft Matter* **2012**, *8*, 7690–7698.
- (35) Rezvantalab, H.; Shojaei-Zadeh, S. Designing patchy particles for optimum interfacial activity. *Phys. Chem. Chem. Phys.* **2014**, *16*, 8283–8293.
- (36) Ruhland, T. M.; Gröschel, A. H.; Ballard, N.; Skelhon, T. S.; Walther, A.; Müller, A. H. E.; Bon, S. A. F. Influence of Janus Particle Shape on Their Interfacial Behavior at Liquid-Liquid Interfaces. *Langmuir* **2013**, *29*, 1388–1394.
- (37) Agrawal, G.; Agrawal, R. Janus Nanoparticles: Recent Advances in Their Interfacial and Biomedical Applications. *ACS Applied Nano Materials* **2019**, *2*, 1738–1757.
- (38) Tu, F.; Lee, D. Shape-Changing and Amphiphilicity-Reversing Janus Particles with pH-Responsive Surfactant Properties. *J. Am. Chem. Soc.* **2014**, *136*, 9999–10006.
- (39) Kadam, R.; Zilli, M.; Maas, M.; Rezwan, K. Nanoscale Janus Particles with Dual Protein Functionalization. *Particle & Particle Systems Characterization* **2018**, 35, 1700332.
- (40) Ballard, N.; Law, A. D.; Bon, S. A. F. Colloidal particles at fluid interfaces: behaviour of isolated particles. *Soft Matter* **2019**, *15*, 1186–1199.
- (41) Maestro, A.; Guzmán, E.; Santini, E.; Ravera, F.; Liggieri, L.; Ortega, F.; Rubio, R. G. Wettability of silica nanoparticle-surfactant nanocomposite interfacial layers. *Soft Matter* **2012**, *8*, 837–843.
- (42) Casagrande, C.; Veyssie, M. Janus beads realization and 1st observation of interfacial properties. C. R. Acad. Sci., Ser. II 1988, 306, 1423–1425
- (43) Ondarcuhu, T.; Fabre, P.; Raphael, E.; Veyssie, M. Specific properties pf amphiphilic particles at fluid interfaces. *J. Phys.* **1990**, *51*, 1527–1536.
- (44) Synytska, A.; Kirillova, A.; Isa, L. Synthesis and Contact Angle Measurements of Janus Particles. *ChemPlusChem* **2014**, *79*, 656–661.
- (45) Stocco, A.; Chollet, B.; Wang, X.; Blanc, C.; Nobili, M. Rotational diffusion of partially wetted colloids at fluid interfaces. *J. Colloid Interface Sci.* **2019**, 542, 363–369.
- (46) Binks, B. P.; Fletcher, P. D. I. Particles Adsorbed at the Oil/Water Interface: A Theoretical Comparison between Spheres of Uniform Wettability and "Janus" Particles. *Langmuir* **2001**, *17*, 4708–4710.
- (47) Borówko, M.; Słyk, E.; Sokołowski, S.; Staszewski, T. Janus Dimers at Liquid-Liquid Interfaces. *J. Phys. Chem. B* **2019**, *123*, 4139–4147.
- (48) Park, B. J.; Lee, D. Equilibrium Orientation of Nonspherical Janus Particles at Fluid-Fluid Interfaces. *ACS Nano* **2012**, *6*, 782–790.
- (49) Fan, H.; Resasco, D. E.; Striolo, A. Amphiphilic Silica Nanoparticles at the Decane-Water Interface: Insights from Atomistic Simulations. *Langmuir* **2011**, 27, 5264–5274.
- (50) Luu, X.-C.; Yu, J.; Striolo, A. Ellipsoidal Janus Nanoparticles Adsorbed at the Water-Oil Interface: Some Evidence of Emergent Behavior. *J. Phys. Chem. B* **2013**, *117*, 13922–13929.
- (51) Sicard, F.; Striolo, A. In *Anisotropic Particle Assemblies*; Wu, N., Lee, D., Striolo, A., Eds.; Elsevier: Amsterdam, 2018; Chapter 6, pp 167–200.

(52) Rezvantalab, H.; Shojaei-Zadeh, S. Capillary interactions between spherical Janus particles at liquid-fluid interfaces. *Soft Matter* **2013**, *9*, 3640–3650.

- (53) Gao, H.-M.; Lu, Z.-Y.; Liu, H.; Sun, Z.-Y.; An, L.-J. Orientation and surface activity of Janus particles at fluid-fluid interfaces. *J. Chem. Phys.* **2014**, *141*, 134907.
- (54) Ballard, N.; Bon, S. A. F. Equilibrium orientations of non-spherical and chemically anisotropic particles at liquid-liquid interfaces and the effect on emulsion stability. *J. Colloid Interface Sci.* **2015**, 448, 533–544.
- (55) Koplik, J.; Maldarelli, C. Molecular dynamics study of the translation and rotation of amphiphilic Janus nanoparticles at a vaporliquid surface. *Physical Review Fluids* **2019**, *4*, 044201.
- (56) Anzivino, C.; Chang, F.; Soligno, G.; van Roij, R.; Kegel, W. K.; Dijkstra, M. Equilibrium configurations and capillary interactions of Janus dumbbells and spherocylinders at fluid-fluid interfaces. *Soft Matter* **2019**, *15*, 2638–2647.
- (57) Kozina, A.; Ramos, S.; Díaz-Leyva, P.; Castillo, R. Bilayers of Janus and homogeneous particle mixtures trapped at an air/water interface. *Soft Matter* **2018**, *14*, 2582–2585.
- (58) Synytska, A.; Khanum, R.; Ionov, L.; Cherif, C.; Bellmann, C. Water-Repellent Textile via Decorating Fibers with Amphiphilic Janus Particles. *ACS Appl. Mater. Interfaces* **2011**, *3*, 1216–1220.
- (59) Sashuk, V.; Holyst, R.; Wojciechowski, T.; Fiałkowski, M. Close-packed monolayers of charged Janus-type nanoparticles at the air-water interface. *J. Colloid Interface Sci.* **2012**, *375*, 180–186.
- (60) Wu, D.; Honciuc, A. Design of Janus Nanoparticles with pH-Triggered Switchable Amphiphilicity for Interfacial Applications. *ACS Applied Nano Materials* **2018**, *1*, 471–482.
- (61) Haney, B.; Chen, D.; Cai, L.-H.; Weitz, D.; Ramakrishnan, S. Millimeter-Size Pickering Emulsions Stabilized with Janus Microparticles. *Langmuir* **2019**, *35*, 4693–4701.
- (62) Adams, D. J.; Adams, S.; Melrose, J.; Weaver, A. C. Influence of particle surface roughness on the behaviour of Janus particles at interfaces. *Colloids Surf.*, A **2008**, 317, 360–365.
- (63) Ruhland, T. M.; Gröschel, A. H.; Walther, A.; Müller, A. H. E. Janus Cylinders at Liquid-Liquid Interfaces. *Langmuir* **2011**, 27, 9807–9814.
- (64) Glaser, N.; Adams, D. J.; Böker, A.; Krausch, G. Janus Particles at Liquid-Liquid Interfaces. *Langmuir* **2006**, *22*, 5227–5229.
- (65) Fernandez-Rodriguez, M. A.; Ramos, J.; Isa, L.; Rodriguez-Valverde, M. A.; Cabrerizo-Vilchez, M. A.; Hidalgo-Alvarez, R. Interfacial Activity and Contact Angle of Homogeneous, Functionalized, and Janus Nanoparticles at the Water/Decane Interface. *Langmuir* 2015, 31, 8818–8823.
- (66) Fernandez-Rodriguez, M. A.; Song, Y.; Rodriguez-Valverde, M. A.; Chen, S.; Cabrerizo-Vilchez, M. A.; Hidalgo-Alvarez, R. Comparison of the Interfacial Activity between Homogeneous and Janus Gold Nanoparticles by Pendant Drop Tensiometry. *Langmuir* **2014**, *30*, 1799–1804.
- (67) Bradley, L. C.; Chen, W.-H.; Stebe, K. J.; Lee, D. Janus and patchy colloids at fluid interfaces. *Curr. Opin. Colloid Interface Sci.* **2017**, *30*, 25–33.
- (68) Fernandez-Rodriguez, M. A.; Rodriguez-Valverde, M. A.; Cabrerizo-Vilchez, M. A.; Hidalgo-Alvarez, R. Surface activity of Janus particles adsorbed at fluid-fluid interfaces: Theoretical and experimental aspects. *Adv. Colloid Interface Sci.* **2016**, 233, 240–254.
- (69) Li, T.; Lilja, K.; Morris, R. J.; Brandani, G. B. Langmuir-Blodgett technique for anisotropic colloids: Young investigator perspective. *J. Colloid Interface Sci.* **2019**, *540*, 420–438.
- (70) Cheung, D. L.; Bon, S. A. F. Stability of Janus nanoparticles at fluid interfaces. *Soft Matter* **2009**, *5*, 3969–3976.
- (71) Wang, X.; In, M.; Blanc, C.; Malgaretti, P.; Nobili, M.; Stocco, A. Wetting and orientation of catalytic Janus colloids at the surface of water. *Faraday Discuss.* **2016**, *191*, 305–324.
- (72) Garbin, V. Collapse mechanisms and extreme deformation of particle-laden interfaces. *Curr. Opin. Colloid Interface Sci.* **2019**, 39, 202–211.

(73) Jaensson, N.; Vermant, J. Tensiometry and rheology of complex interfaces. *Curr. Opin. Colloid Interface Sci.* **2018**, 37, 136–150.

- (74) Mendoza, A. J.; Guzmán, E.; Martínez-Pedrero, F.; Ritacco, H.; Rubio, R. G.; Ortega, F.; Starov, V. M.; Miller, R. Particle laden fluid interfaces: Dynamics and interfacial rheology. Advances in Colloid and Interface. *Adv. Colloid Interface Sci.* **2014**, *206*, 303–319.
- (75) Rashidi, A.; Issa, M. W.; Martin, I. T.; Avishai, A.; Razavi, S.; Wirth, C. L. Local Measurement of Janus Particle Cap Thickness. ACS Appl. Mater. Interfaces 2018, 10, 30925–30929.
- (76) Mendoza, A. J.; Guzmán, E.; Martínez-Pedrero, F.; Ritacco, H.; Rubio, R. G.; Ortega, F.; Starov, V. M.; Miller, R. Particle laden fluid interfaces: Dynamics and interfacial rheology. *Adv. Colloid Interface Sci.* **2014**, *206*, 303–319.
- (77) Gopal, A.; Lee, K. Y. C. Headgroup Percolation and Collapse of Condensed Langmuir Monolayers. *J. Phys. Chem. B* **2006**, 110, 22079–22087.
- (78) Lee, K. Y. C.; Lipp, M. M.; Takamoto, D. Y.; Ter-Ovanesyan, E.; Zasadzinski, J. A.; Waring, A. J. Apparatus for the Continuous Monitoring of Surface Morphology via Fluorescence Microscopy during Monolayer Transfer to Substrates. *Langmuir* **1998**, *14*, 2567–2572.
- (79) Razavi, S.; Kretzschmar, I.; Koplik, J.; Colosqui, C. E. Nanoparticles at liquid interfaces: Rotational dynamics and angular locking. *J. Chem. Phys.* **2014**, *140*, 014904.
- (80) Razavi, S.; Koplik, J.; Kretzschmar, I. The effect of capillary bridging on the Janus particle stability at the interface of two immiscible liquids. *Soft Matter* **2013**, *9*, 4585–4589.
- (81) Razavi, S.; Koplik, J.; Kretzschmar, I. Molecular Dynamics Simulations: Insight into Molecular Phenomena at Interfaces. *Langmuir* **2014**, *30*, 11272–11283.
- (82) Razavi, S. Janus Colloidal Particles and Fluid Interfaces: Approach, Breach, And Flow Behavior. Ph.D. Dissertation, The City College of New York, 2015.
- (83) Razavi, S.; Cao, K. D.; Lin, B.; Lee, K. Y. C.; Tu, R. S.; Kretzschmar, I. Collapse of Particle-Laden Interfaces under Compression: Buckling vs Particle Expulsion. *Langmuir* **2015**, *31*, 7764–7775.
- (84) Miller, K.; Tsyrenova, A.; Anthony, S. M.; Qin, S.; Yong, X.; Jiang, S. Drying mediated orientation and assembly structure of amphiphilic Janus particles. *Soft Matter* **2018**, *14*, *6793*–*6798*.
- (85) Kumar, A.; Park, B. J.; Tu, F.; Lee, D. Amphiphilic Janus particles at fluid interfaces. *Soft Matter* **2013**, *9*, 6604–6617.
- (86) Botto, L.; Lewandowski, E. P.; Cavallaro, M.; Stebe, K. J. Capillary interactions between anisotropic particles. *Soft Matter* **2012**, *8*, 9957–9971.
- (87) Park, B. J.; Choi, C.-H.; Kang, S.-M.; Tettey, K. E.; Lee, C.-S.; Lee, D. Geometrically and chemically anisotropic particles at an oil-water interface. *Soft Matter* **2013**, *9*, 3383–3388.
- (88) Chio, C. C.; Tse, Y.-L. S. Patchy colloidal particles at the fluid-fluid interface. *Soft Matter* **2018**, *14*, 9457–9465.
- (89) Rezvantalab, H.; Drazer, G.; Shojaei-Zadeh, S. Molecular simulation of translational and rotational diffusion of Janus nanoparticles at liquid interfaces. *J. Chem. Phys.* **2015**, *142*, 014701.
- (90) Israelachvili, J. N.; Wennerstroem, H. Entropic forces between amphiphilic surfaces in liquids. *J. Phys. Chem.* **1992**, *96*, 520–531.
- (91) Israelachvili, J. N. Intermolecular and Surface Forces, 3rd ed.; Academic Press: Boston, 2011.
- (92) Ranade, M. B. Adhesion and Removal of Fine Particles on Surfaces. *Aerosol Sci. Technol.* **1987**, *7*, 161–176.
- (93) Park, B. J.; Brugarolas, T.; Lee, D. Janus particles at an oil-water interface. *Soft Matter* **2011**, *7*, 6413–6417.
- (94) Lenis, J.; Razavi, S.; Cao, K. D.; Lin, B.; Lee, K. Y. C.; Tu, R. S.; Kretzschmar, I. Mechanical Stability of Polystyrene and Janus Particle Monolayers at the Air/Water Interface. *J. Am. Chem. Soc.* **2015**, *137*, 15370–15373.
- (95) Trevor, D. J.; Chidsey, C. E. D. Room temperature surface diffusion mechanisms observed by scanning tunneling microscopy. *J. Vac. Sci. Technol., B: Microelectron. Process. Phenom.* 1991, 9, 964–968.

(96) Trevor, D. J.; Chidsey, C. E. D.; Loiacono, D. N. In Situ Scanning-Tunneling-Microscope Observation of Roughening, Annealing, and Dissolution of Gold (111) in an Electrochemical Cell. *Phys. Rev. Lett.* **1989**, *62*, 929–932.

- (97) McCarley, R. L.; Dunaway, D. J.; Willicut, R. J. Mobility of the alkanethiol-gold (111) interface studied by scanning probe microscopy. *Langmuir* **1993**, *9*, 2775–2777.
- (98) Vigil, G.; Xu, Z.; Steinberg, S.; Israelachvili, J. Interactions of Silica Surfaces. *J. Colloid Interface Sci.* **1994**, *165*, 367–385.